X-ray Diffraction, EPR, and ^{6}Li and ^{27}Al MAS NMR Study of $LiAlO_2$−$LiCoO_2$ Solid Solutions

R. Alcántara, P. Lavela, P. L. Relaño, and J. L. Tirado*

Laboratorio de Química Inorgánica, Facultad de Ciencias, Universidad de Córdoba, Avda. San Alberto Magno s/n, 14004 Córdoba, Spain

E. Zhecheva and R. Stoyanova

Institute of General and Inorganic Chemistry, Bulgarian Academy of Sciences, 1113 Sofia, Bulgaria

Received June 12, 1997[⊗]

The preparation of solid solutions of the $LiAlO_2$−$LiCoO_2$ system in the complete composition range is described. Powder X-ray diffraction gives direct information about the partial substitution of Co by Al atoms, together with a fractional occupancy of tetracoordinated sites by aluminum atoms. EPR of impurity Ni^{3+} ions and ^{6}Li and ^{27}Al MAS NMR spectroscopies are used to assess for cation distribution. ^{6}Li NMR spectra show a single resonance of lithium ions in octahedral sites. ^{27}Al NMR spectra show that the distribution of Al atoms in tetrahedral and octahedral sites changes with composition. EPR spectra evidence that Ni^{3+} impurity ions in the $Al_yCo_{1-y}O_2$ layers prefer mainly Al^{3+} ions as first neighbors. The potential applicability of these materials as intercalation electrodes is also evaluated in lithium anode cells. A poor lithium ion diffusivity, resulting from the presence of aluminum in both tetrahedral and octahedral sites, may limit the applicability of $LiAl_yCo_{1-y}O_2$ cathodes. The partial substitution of Co by Ni leads to an improvement of the electrochemical performance.

Introduction

Several ternary oxides of general formula $LiMO_2$ exhibit interesting properties and technological applications. The catalytic properties of both the acidic and basic sites of $LiAlO_2$ was recently examined, and the unique activity of the α form has been explained in terms of the formation of Li^+...H^- aducts.[1] Lithium ion replacement by protons in α-$LiAlO_2$ was shown to yield "$HAlO_2$",[2] which after calcination showed active basic sites for acetone aldol condensation reactions. For $LiCoO_2$, the lithium ion replacement by protons to give the isostructural $HCoO_2$ has also been reported.[3]

On the other hand, the structure and electrochemical properties of $LiNiO_2$[4,5] and $LiCoO_2$[6,7] oxides and their solid solutions[8,9] have been studied in detail in the last decade, due to their interest as positive electrodes in lithium and lithium ion cells. One of the most important limitations associated with the use of Li_x-CoO_2 cathodes comes from the thermodynamic instability of the fully deintercalated solid with CoO_2 stoichiometry and layered structure. Until very recently, it was thought that x values lower than 0.4 always lead to the collapse of the layered structure prior to the complete lithium extraction.[6,7] The large potential required for the complete electrochemical extraction of lithium from $LiCoO_2$ also made this process difficult to observe due to the low stability of most common electrolytes under these conditions. However, the formation of an O1 (CdI_2-type) layered CoO_2 phase was recently reported.[10] In addition, other complex structural transitions occur for x values in the 1.0−0.4 range. A strong first-order transition takes place at $0.75 < x < 0.93$, which may also limit the reversibility of the intercalation−deintercalation process. The occurrence of a monoclinic modification takes place near $x = 0.5$ by ordering of the lithium ions. Finally, a third structural modification is found in the $0.3 < x < 0.5$ range.[7] The changes in lattice dimensions during the insertion−extraction processes induce internal strains due to the mismatch between the zones with a different degree of intercalation in the solid. These in turn lead to a highly stressed solid, which develops cracks followed by particle fragmentation, which destroys the crystallinity of the matrix solid and hence the cyclability of the cell. In order to overcome this effect different approaches have been followed. One of them consists of the introduction of other ions into the structure which may stabilize the layered solid with or without participating in the redox processes. For these purposes different isostructural oxides may provide appropriate solid solutions with $LiCoO_2$.

$LiCrO_2$, $LiCoO_2$, $LiNiO_2$, and α-$LiAlO_2$ possess the layered structure of α-$NaFeO_2$ which results from monovalent and trivalent cation ordering in the octahedral sites of alternate

[⊗] Abstract published in *Advance ACS Abstracts,* December 15, 1997.

(1) Tomczak, D. C.; Allen, J. L.; Poeppelmeier, K. R. *J. Catal.* **1994**, *146*, 155.
(2) Poeppelmeier, K. R.; Kipp, D. O. *Inorg. Chem.* **1988**, *27*, 767.
(3) Fernández, J. M.; Hernán, L.; Morales, J.; Tirado, J. L. *Mater. Res. Bull.* **1988**, *23*, 899.
(4) Dahn, J. R.; von Sacken, U.; Juzkow, M. W.; Al-Janaby, H. *J. Electrochem. Soc.* **1991**, *138*, 2207.
(5) Ohzuku, T.; Ueda, A.; Nagayama, M. *J. Electrochem. Soc.* **1993**, *140*, 1862.
(6) Mizushima, K.; Jones, P. C.; Wiseman, P. J.; Goodenough, J. B. *Mater. Res. Bull.* **1980**, *15*, 783.
(7) Reimers, J. N.; Dahn, J. R. *J. Electrochem. Soc.* **1992**, *139*, 2091.
(8) Ueda, A.; Ohzuku, T. *J. Electrochem. Soc.* **1994**, *141*, 2010.
(9) Marichal, C.; Hirshinger, J.; Granger, P.; Ménétrier, M.; Rougier, A.; Delmas, C. *Inorg. Chem.* **1995**, *34*, 1773.
(10) Amatucci, G. G.; Tarascon, J. M.; Klein, L. C. *J. Electrochem. Soc.* **1996**, *142*, 1114.

S0020-1669(97)00722-2 CCC: $15.00
Published on Web 01/26/1998

interlayers defined by oxygen anions in a nearly cubic closest packing. The resulting trigonal space group is $R\bar{3}m$ with Li, M, and O atoms at equivalent sites 3b, 3a, and 3c, respectively. Poeppelmeier and Thong[11] synthesized $LiCrO_2$−$LiAlO_2$ solid solutions in which the α-structure was preserved for Al/(Al + Cr) ≥ 0.6. Recently, Zhong and von Sacken[12] and Ohzuku et al.[13] studied the compound with composition $LiAl_{1/4}Ni_{3/4}O_2$ and $R\bar{3}m$ structure. In the present work, the formation of $LiAlO_2$−$LiCoO_2$ solid solutions is studied.

Experimental Section

Powder samples of nominal composition $LiAl_yCo_{1-y}O_2$ were prepared by the following procedure. Solutions (1 M) of $Al(NO_3)_3 \cdot 9H_2O$ (Panreac), $Co(CH_3COO)_2$, and LiOH (Merck) were mixed in the desired proportions, and the solvent was evaporated at ca. 373 K. The solid residue was thermally treated for a 24-h period at 673 K. The product was then pressed into 7 mm diameter pellets at ca. 4 tons and then heated at 973 K for 7 days. Attempts to obtain this material by the careful mixture and homogenization of $LiCoO_2$ and α-$LiAlO_2$ powders followed by pelletization and thermal treatment at 673 (24 h), 773 (24 h), and 973 K (30 h) were unsuccessful. $LiCoO_2$ and α-$LiAlO_2$ were prepared according to previously reported procedures.[2,7] A sample of $LiAl_{0.16}Ni_{0.71}Co_{0.13}O_2$ stoichiometry was prepared as follows. Stoichiometric amounts of $Ni(OH)_2$, $CoCO_3$, and $Al(NO_3)_3$ (Merck) were dissolved in a 0.5 M aqueous solution of citric acid, reaching a (Ni + Co + Al)/citric = 1:1 molar ratio. LiOH (Merck) was added, reaching a Li/citric = 1:1 molar ratio. The resulting solution was freeze-dried in an Alpha-Crist freeze-dryer apparatus. The solid residue was thermally treated at 773 K for 1 h. The product was then heated at 973 K under oxygen flow for two 24-h periods, with intermediate grinding.

Room temperature ^{6}Li and ^{27}Al MAS NMR spectra were recorded on a Bruker ACP-400 spectrometer working at 58.89 and 104.26 MHz resonance frequencies, respectively (9.400 T), and at a 5-kHz spinning rate. The aluminum spectra were referenced to an acidified 1 M solution of $Al(NO_3)_3$. The lithium spectra were referenced to a 1 M LiCl aqueous solution.

EPR spectra were registered as the first derivative of the absorption signal with an ERS-220/Q spectrometer (ex-GDR) within the temperature range between 90 and 400 K. The *g* factors were established with respect to a Mn^{2+}/ZnS standard. The signal intensity was determined by double integration of the experimental EPR spectrum. Recordings at different microwave power were used to distinguish the EPR signals.

X-ray powder diffraction data (XPD) were obtained with a Siemens D5000 apparatus provided with Cu Kα radiation and a graphite monochromator. Step−scan recordings for structure refinement by the Rietveld method were carried out by using 0.04° 2Θ steps of 6-s duration. The computer program DBWS9000 was used in the calculations.[14]

The electrochemical performance of Li/$LiClO_4$(PC + EC)/mixed oxide test cells was studied in galvanostatic and potentiostatic modes by using alternatively an Amel apparatus and a multichannel MacPile system.[15] Cell cathodes were prepared by pressing, at ca. 5 tons, a mixture of 40% graphite and mixed oxide. Step potential electrochemical spectroscopy (SPES) was carried out with 10 mV/h steps after an initial relaxation of the cell until the condition $\Delta V/\Delta t$ < 1 mV/h was reached. Intensiostatic cycling was performed in the as-prepared cells at C/50 (i.e., allowing a $\Delta x = 1$ in Li_xCoO_2 in 50 h).

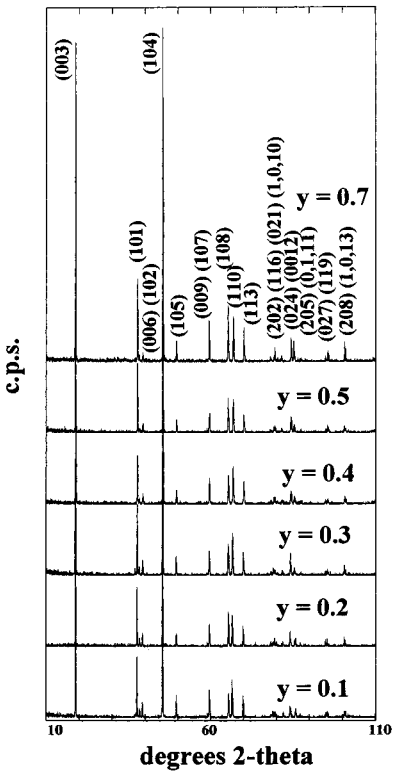

Figure 1. Powder X-ray diffraction data of $LiAl_yCo_{1-y}O_2$ samples.

Table 1. Unit Cell Parameters of $LiAl_yCo_{1-y}O_2$ Samples

y	*a* (Å)	*c* (Å)	*c*/*a*
0.10	2.8125(2)	14.088(1)	5.009
0.20	2.8134(1)	14.0685(5)	5.001
0.30	2.8108(3)	14.137(1)	5.030
0.50	2.8000(2)	14.178(1)	5.064
0.70	2.8008(2)	14.1960(7)	5.069

Results and Discussion

The XPD patterns of powdered $LiAl_yCo_{1-y}O_2$ were all indexable in the $LiCoO_2$ or α-$LiAlO_2$ rhombohedral structure (Figure 1). The values of the unit cell parameters are included in Table 1. For the limiting compositions, $y = 0$ and $y = 1$, the unit cell parameters were coincident with those previously reported in the literature for similar preparation temperatures.[2,7] It should be noted that the unit cell parameters of both α-$LiAlO_2$ and $LiCoO_2$ are highly coincident, which is consistent with the similarity of the trivalent metal ionic radii[16] $r_{Al^{3+}CN=6} = 68$ pm, $r_{Co^{3+}CN=6,LS} = 69$ pm for Co^{3+} in a low-spin configuration and Al^{3+}. The resulting changes of lattice parameters for intermediate $LiAl_yCo_{1-y}O_2$ compositions are small and make it difficult to discern a clear trend that could be indicative of a simple metal substitution phenomenon in these solid solutions. This result contrasts with the findings for other related systems such as the $LiCrO_2$−$LiAlO_2$ solid solutions,[11] in which the end members differ significantly in their unit cell parameters and the intermediate compositions showed a linear change, in agreement with Vegard's law. In order to discern the true cation distribution, the Rietveld analysis of selected powder X-ray diffraction patterns was carried out in the $R\bar{3}m$ space group. By using hexagonal axes, the unit cell origin was fixed at center

(11) Poeppelmeier, K. R.; Thong, S. H. *J. Less-Common Met.* **1989**, *156*, 291.
(12) Zhong, Q.; von Sacken, U. *J. Power Sources* **1995**, *54*, 221.
(13) Ohzuku, T.; Ueda, A.; Kouguchi, M. *J. Electrochem. Soc.* **1995**, *142*, 4033.
(14) Young, R. A.; Wiles, D. B. *J. Appl. Crystallogr.* **1982**, *15*, 430.
(15) (a) Chabre, Y. *J. Electrochem. Soc.* **1991**, *138*, 329. (b) Chabre, Y.; Djurado, D.; Armand, M.; Romanow, W. R.; Coustel, N.; McCauley, J. P.; Fischer, J. E.; Smith, A. B. *J. Am. Chem. Soc.* **1992**, *114*, 764. (c) Morales, J.; Stoyanova, R.; Tirado, J. L.; Zhecheva, E. *J. Solid State Chem.* **1994**, *113*, 182. (d) Alcántara, R.; Morales, J.; Tirado, J. L.; Stoyanova, R.; Zhecheva, E. *J. Electrochem. Soc.* **1995**, *142*, 3997.
(16) Shannon, R. D. *Acta Crystallogr.* **1976**, *A32*, 751.

Table 2. Results of the Rietveld Refinement of Powder X-ray Diffraction Data for $LiAl_{0.2}Co_{0.8}O_2$

formula	$LiAl_{0.2}Co_{0.8}O_2$
space group	$R\bar{3}m$
hexagonal axes	
a, Å	2.8134(1)
c, Å	14.0685(5)
Z	3
temp, K	298
radiation	Cu Kα
2θ limits, deg	10−110
R_B	3.71
S (R_w/R_e)	0.35

		fractional coordinate			
atom	site	x	y	z	occupancy
Li	3b	0.0	0.0	0.5	1
Co	3a	0.0	0.0	0.0	0.8
Al(1)	3a	0.0	0.0	0.0	0.139
Al(2)	6c	0.0	0.0	0.1383(2)	0.061
O	6c	0.0	0.0	0.2594(1)	2.0

3m, with Li and O at 3b and 6c sites ($z = 0.25-0.26$), respectively. In a first approach, Al and Co ions were statistically distributed in 3a sites. The results obtained for $LiAl_yCo_{1-y}O_2$ compositions in the $y = 0.1-0.3$ range never allowed acceptable R_{Bragg} values to be reached by using this simple model. Thus, the possible changes in coordination of aluminum were tested by allowing a partial occupancy of 6c sites by Al atoms in the Rietveld refinement. The refined parameters and R values obtained by this procedure for $y = 0.2$ are included in Table 2. The occupancy of 6c sites with $z \approx 0.14$ by aluminum atoms is significant. The location of aluminum ions in pseudotetrahedral coordination is not surprising, as other lithium aluminum mixed oxides with structures derived from a cubic closest packing of oxygen atoms, such as $LiAl_5O_8$,[17] have tetrahedrally coordinated Al. Aluminum contents larger than 0.3 resulted in a poorer fitting according to the latter model, probably due to a significantly lower proportion of aluminum in pseudotetrahedral sites. The complementary information about the local environment of the aluminum obtained from spectroscopic measurements for these materials is in good agreement with the interpretation given to the X-ray diffraction results, as shown below.

The ^6Li and ^{27}Al MAS NMR spectra of the solid solutions are shown in Figure 2A,C. For the end members, $LiCoO_2$ and $LiAlO_2$, and the solid solutions $LiAl_yCo_{1-y}O_2$, the ^6Li spectra showed a single resonance line at ca. 0 ppm as referred to aqueous 1 M LiCl solutions and the corresponding spinning side bands (Figure 2A). This means that the lithium atoms occupy the six-coordinated crystal sites and the chemical shift is not sensitive to the interactions of ^6Li with ^{27}Al and ^{59}Co nuclei. It should be noted that Marichal et al.[9] have found that lithium MAS NMR spectra in the −80−0 ppm region provided relevant structural information on $LiNi_{1-y}Co_yO_2$ solid solutions, as a result of the interactions of ^6Li nuclei with the Ni^{3+} ions in the second coordination sphere. The diamagnetic Al^{3+} and Co^{3+} ions do not allow a similar effect, and thus the spectra cannot be used to obtain information about site distribution probabilities. The ^6Li spectra of $LiAl_5O_8$ reported by Stewart et al.[17] also showed a single resonance which was considered the result of the same oxygen coordination number of lithium, irrespective of the presence of aluminum in tetrahedral and octahedral sites.

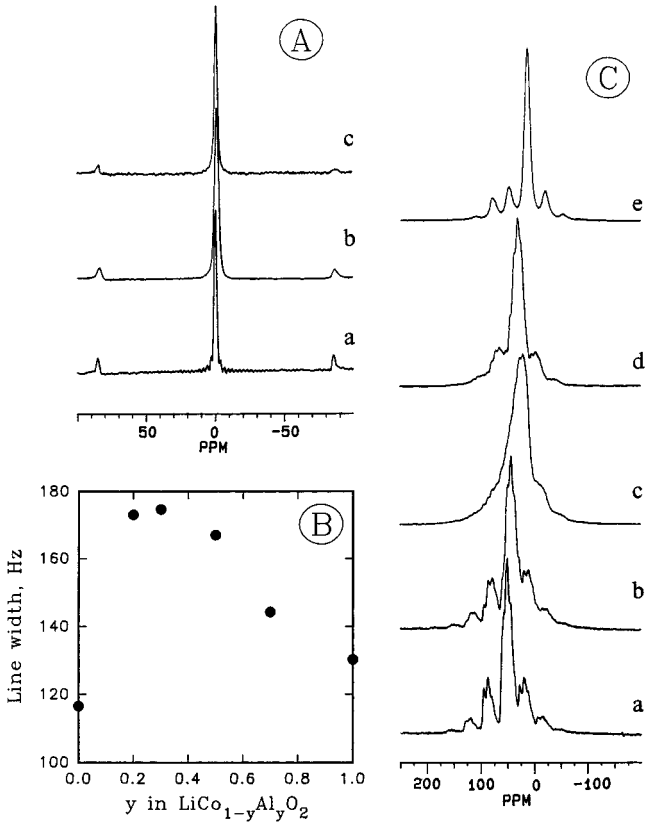

Figure 2. (A) ^6Li MAS NMR spectra of (a) $LiCoO_2$, (b) $LiAl_{0.3}Co_{0.7}O_2$, and (c) $LiAlO_2$. (B) Line width of the main resonance ^6Li peak versus aluminum content in $LiAl_yCo_{1-y}O_2$. (C) ^{27}Al MAS NMR spectra of $LiAl_yCo_{1-y}O_2$ solid solutions with (a) $y = 0.2$, (b) $y = 0.3$, (c) $y = 0.5$, and (d) $y = 0.7$ and (e) $LiAlO_2$.

The parameter that only changes in the ^6Li NMR spectra is the line width of the main resonance peak (Figure 2B). Increasing aluminum content up to 30 atom % causes a marked increase in the line width of ^6Li resonance peak, while a further increase in the aluminum content produces a narrowing of the ^6Li resonance peak. In addition, the line width of ^6Li resonance peak is nearly the same for the pure $LiCoO_2$ and $LiAlO_2$. The line broadening observed for ^{27}Al-doped $LiCoO_2$ suggests that the lithium ions reside in unequivalent octahedral sites which are distinguished by the slightly dissimilar degree of distortion resulting from the different occupancy of neighbor sites by cobalt and aluminum.

The analysis of ^{27}Al NMR data was carried out to obtain complementary information about the local environment of aluminum atoms. The presence of AlO_4 and AlO_6, and more recently aluminum pentacoordinated by oxygen, has been resolved in crystalline and amorphous materials and minerals.[17−24] However, the interpretation of ^{27}Al NMR spectra is complicated by the quadrupolar interaction resulting from the spin $I = 5/2$. MAS measurements can only average efficiently first-order

(17) Stewart, F. F.; Stebbins, J. F.; Peterson, E. S.; Farnan, Y.; Dunham, S. O.; Adams, E.; Jennings, P. W. *Chem. Mater*. **1995**, *7*, 363.
(18) Dec, S. F.; Maciel, G. E.; Fitzgerald, J. J. *J. Am. Chem. Soc*. **1990**, *112*, 9069.
(19) Weller, M. T.; Brenchley, M. E.; Apperley, D. C.; Davies, N. A. *Solid State Nucl. Magn. Reson.* **1994**, *3*, 103.
(20) Simon, S.; van der Pol, A.; Reijerse, E. J.; Kentgens, A. P. M.; van Moorsel G. J.; de Boer, E. *J. Chem. Soc., Faraday Trans.* **1994**, *90*, 2663.
(21) Chee, K. S.; Cheng, Y. B.; Smith, M. E. *Chem. Mater*. **1995**, *7*, 982.
(22) Shi, J.; Anderson, M. A.; Carr, S. W. *Chem. Mater*. **1996**, *8*, 369.
(23) Lippmaa, E.; Samoson, A.; Mägi, M. *J. Am. Chem. Soc*. **1986**, *108*, 1730.
(24) Smith, M. E.; Steuernagel, S. *Solid State Nucl. Magn. Reson.* **1992**, *1*, 175.

broadening effects. Second-order effects—enhanced broadening of the resonances and shift of peak position from the isotropic chemical shift—are present, yielding poorer resolution and asymmetric lines with a tail to negative shift. Nevertheless, Stewart et al.[17] have shown that the ^{27}Al MAS NMR spectra provided more structural information than the ^{6}Li or ^{7}Li spectra of $LiAl_5O_8$. In the analysis reported by Weller et al.[19] on the correlation between the chemical shift of the ^{27}Al resonance frequency and the Al−O−Al angle of the distorted tetrahedra, a 75−80 ppm window was observed. The resonances at 0−8 ppm and 58−64 ppm are unambiguously accepted to originate from hexa- and tetracoordinated Al, respectively, while resonances at ca. 30 ppm can be ascribed to pentacoordinated Al.

Taking into account the trigonal structure of $LiAlO_2$, one can expect that the second-order quadrupole effects will only perturb the ^{27}Al spectrum. The ^{27}Al MAS NMR spectrum of pure α-$LiAlO_2$ or α-$LiAlO_2$ intimately mixed with $LiCoO_2$ powders consists of one broad signal at 15 ppm with a pair of spinning side bands (Figure 2Ce), which is typical for hexacoordinated Al. Drastic changes in the ^{27}Al spectrum are observed for Al-substituted $LiCoO_2$. The ^{27}Al MAS NMR spectra of $LiAl_yCo_{1-y}O_2$ show complex center bands including several equidistant Gaussians with line widths of 5−6 ppm (Figure 2Ca−d). The distribution of the band intensities depends on the aluminum content. At 20% of Al, the most intensive band is located at about 65 ppm. As the aluminum content increases, the position of the intensive peak is located from 65 to 15 ppm. This peak displacement reflects the changes in the local structure of Al. The shape of the complex profile of the intensive peak was found to be unaffected by the spinning rate. The appearance of the bands between 15 and 65 ppm can be interpreted not only by the second-order quadrupole effects but also by the coupling between Al in hexa- and tetracoordination. In addition, the spinning side bands are inside the range of the two bands at 15 and 65 pm (Figure 2C). From the analysis of the ^{27}Al NMR spectra, it can be inferred that aluminum occupies both the tetra- and hexacoordinated sites, the ratio between them depending on the total aluminum content. For Al-poor compositions, aluminum prefers tetra- instead of hexacoordination, while for Al-rich compositions, aluminum tends to fill the hexacoordinated sites. The appearance of tetracoordinated Al in trigonal $LiAl_yCo_{1-y}O_2$ is not consistent with the Rietveld refinement data concerning the statistical distribution of Co and Al in octahedral 3b sites. This result is not surprising if we consider the different scattering factors for Al and Co. This indicates that the amount of Al is not enough to induce the corresponding changes in XRD patterns.

Owing to the close chemical properties of cobalt and nickel, the main impurity in cobalt salts is usually nickel in concentrations of 0.3−0.5 atom %. Attempting to explore the bond character and cationic distribution in Al-substituted $LiCoO_2$, EPR of low/spin Ni^{3+} ions used as tracers was undertaken. As was shown in previous studies,[25] between 30 and 400 K the EPR spectrum of Ni^{3+} impurity atoms in $LiCoO_2$ consists of a single Lorentzian line with $g = 2.142$. Due to the Jahn−Teller effect, below 30 K the Lorentzian line is transformed into a singlet with a Gaussian shape and a doublet, corresponding to the transitions in the ground vibronic double state of Ni^{3+}.[25] The addition of aluminum to $LiCoO_2$ causes essential changes

(25) (a) Angelov, S.; Friebel, C.; Zhecheva, E.; Stoyanova, R. *J. Phys. Chem. Solids* **1992**, *53*, 443. (b) Stoyanova, R.; Zhecheva, E.; Friebel, C. *J. Phys. Chem. Solids* **1993**, *54*, 9. (c) Stoyanova, R.; Zhecheva, E.; Angelov, S. *Solid State Ionics* **1993**, *59*, 17. (d) Stoyanova, R.; Zhecheva, E.; Alcántara, R.; Lavela, P.; Tirado, J. L. *Solid State Commun.* **1997**, *102*, 457.

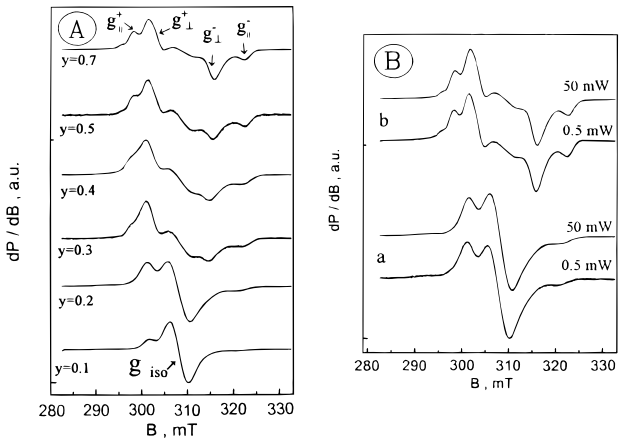

Figure 3. (A) EPR spectra at 113 K of impurity Ni^{3+} in $LiAl_yCo_{1-y}O_2$ samples. (B) Microwave power dependence of the EPR spectrum of impurity Ni^{3+} for (a) $y = 0.30$ and (b) $y = 0.70$.

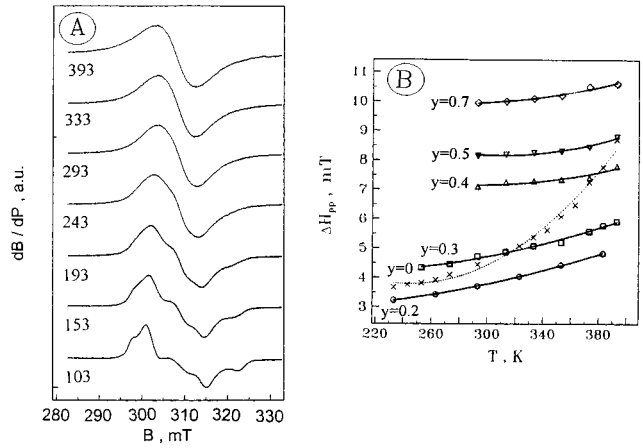

Figure 4. (A) Temperature evolution of the EPR spectrum of impurity Ni^{3+} in $LiAl_{0.70}Co_{0.30}O_2$. (B) Temperature dependence of the EPR Lorentzian line width for $LiAl_yCo_{1-y}O_2$ samples.

in the EPR spectrum of the Ni^{3+} impurity ions. Already at 100 K, the EPR spectrum of Ni^{3+} impurity atoms in aluminum-rich oxides is a superposition of two kinds of signals: a single Gaussian line with $g = 2.140$ and an axially symmetrical doublet with $g_\perp = 2.146$ and $g_{||} = 2.137$ (Figure 3A). When the aluminum content decreases, the additional Lorentzian line, superimposed on the two kinds of EPR signals, grows in intensity (Figure 3A). These signals are distinguished by the microwave power (Figure 3B), as their intensities are affected to different extents.

On heating, the EPR spectrum, consisting of a singlet and a doublet, merges into a single Lorentzian line with $g = 2.142$ (Figure 4A), the averaging temperature, that is, the temperature at which the singlet and the doublet signals coalesce, being dependent on the amount of aluminum. The line width of the Lorentzian curve depends on the recording temperature and the aluminum content (Figure 4B). In agreement with the EPR study of Ni^{3+} in $LiCoO_2$, the singlet and the doublet can be assigned to Jahn−Teller Ni^{3+} species in a trigonally distorted octahedral field: the doublet corresponds to transitions occurring in the ground vibronic doublet state, while the singlet is the relaxation-averaged part of the doublet. The difference between the values of $g_\perp = 2.146$ and $g_{||} = 2.136$ for Ni^{3+} in Al-doped oxides is larger than that for Ni^{3+} in pure $LiCoO_2$ ($g_\perp = 2.141$, $g_{||} = 2.138$), which is associated with the higher degree of trigonal unit cell distortion. In addition, the temperature of averaging the complex EPR spectrum drastically rises with Al-

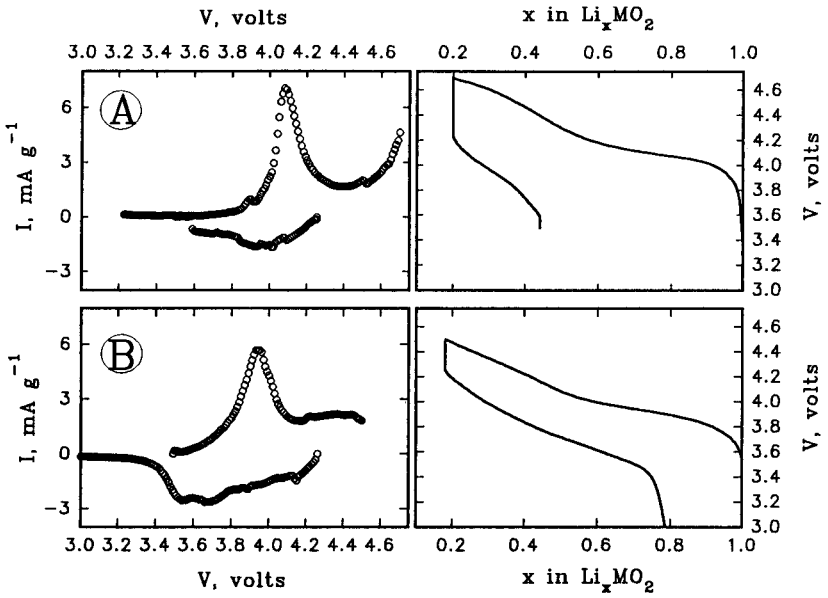

Figure 5. Step potential electrochemical spectroscopy (SPES) results (cell current I vs V plot and V vs composition plot) of (A) $Li/LiClO_4$(PC + EC)/$Li_xAl_{0.2}Co_{0.8}O_2$ test cells and (B) $Li/LiClO_4$(PC + EC)/$Li_xAl_{0.16}Ni_{0.71}Co_{0.13}O_2$ test cells.

containing samples: from 30 K for pure $LiCoO_2$ to 270 K for $LiAl_yCo_{1-y}O_2$. This clear distinction in the averaging temperature can be explained in terms of covalency of the $Ni^{3+}-O^{2-}$ bond changed by Al substitution. It is to be pointed out that when the **g** tensor of an axially symmetrical doublet is independent of the aluminum amount, the degree of trigonal distortion increases smoothly. From this it can be inferred that Ni^{3+} impurity ions in the $Al_yCo_{1-y}O_2$ layers prefer mainly Al^{3+} ions as first neighbors. If a distribution of Al with respect to Co similar to that around the Ni probe atom ions is assumed, the nonuniform distribution could affect the entire $Al_yCo_{1-y}O_2$ layers. In addition, the nonuniform distribution of Al in the vicinity of Ni^{3+} causes a slight dependence of the Lorentzian line on the recording temperature (Figure 4B) but does not result in selective broadening of the X-ray diffraction lines. Hence, the clustering of Al in $LiCoO_2$ covers the microscale regions around Ni^{3+} ions.

Although a detailed characterization of battery performance is not the main objective of this work, the preliminary results on the electrochemical performance of $LiAl_yCo_{1-y}O_2$ solids as active cathode material in lithium anode cells are summarized below. The performance of $LiAl_yCo_{1-y}O_2$ was evaluated for low y values ($y < 0.5$), as larger aluminum contents are not interesting in terms of cell capacity, as compared with Li_xCoO_2 electrodes. The SPES data for $y = 0.2$ are shown in Figure 5A, in which the maximum extraction of lithium is almost equivalent to the complete oxidation of Co^{3+} to Co^{4+}, simultaneous to the extraction of ca. 0.8 lithium ions, provided that no other side reaction is admitted. The intensity vs voltage data reveals a main oxidation peak located at 4.05 V during cell charge which can be ascribed to the first-order transition from $LiAl_yCo_{1-y}O_2$ to $Li_xAl_yCo_{1-y}O_2$ as found for pure $LiCoO_2$.[7] The occurrence of a low-intensity peak at ca. 4.5 V may be indicative of the order−disorder transformations previously found in the electrochemical performance of Li_xCoO_2 cathode cells for x close to 0.5.[7] However, the position of the peak at ca. 4.5 V is significantly higher than that reported for pure Li_xCoO_2, which may be indicative of a slow kinetics of lithium ordering in the interlayer space which polarizes the cell, as discussed below. The increase in cell current which is evident in Figure 5A for voltage values higher than 4.6 V may be ascribed to the first steps of an electrolyte decomposition process. However, the interference of this process on the evaluation of the maximum lithium extraction (minimum x value) is not high (Figure 5A). Thus it can be concluded that the presence of aluminum in the composition of the solid stabilizes the rhombohedral structure, thus allowing a more extended lithium extraction than in pure $LiCoO_2$.

On the other hand, the reversibility of the lithium extraction−intercalation process is poor, as evidenced by the enhanced polarization found for the first cycle of charge−discharge (Figure 5A). This effect is more marked in this solid than in stoichiometric $LiCoO_2$ prepared at the same temperature and can be considered as a consequence of a poorer lithium ion diffusivity, resulting from the presence of aluminum in both tetrahedral and octahedral sites, as discussed above. In turn, these effects may limit the applicability of $LiAl_yCo_{1-y}O_2$ cathodes. In order to overcome this problem, it was taken into account that pure $LiNiO_2$ commonly displays a more extended reversible deintercalation than $LiCoO_2$. Moreover, Ohzuku et al.[13] recently reported a partial improvement of the electrochemical performance of $LiNiO_2$ cathodes by aluminum substitution in $LiAl_yNi_{1-y}O_2$ solid solutions. With these results in mind, nickel was incorporated in the stoichiometry of the Li−Al−Co−O solid solutions by using the preparative procedure described in the Experimental Section, which uses amorphous citrate precursors. Similar procedures have been successfully applied to $LiCoO_2$[26] and $LiNiO_2$.[27] Thus, the quaternary system with $LiAl_{0.16}Ni_{0.71}Co_{0.13}O_2$ stoichiometry was prepared at 973 K and studied in lithium anode cells. Unfortunately, due to the high content in paramagnetic Ni^{3+} ions, the NMR spectra of the quaternary phase did not allow a clear assessment on the location of Al atoms. Nevertheless, the unit cell parameters (a = 2.8596 Å, c = 14.168 Å) reveal a less marked trigonal distortion (c/a = 4.950) as compared with the results in Table 1. The similarity between the unit cell parameters of $LiAl_{0.16}$-

(26) Alcántara, R.; Gorova, M.; Morales, J.; Stoyanova, R.; Tirado, J. L.; Zhecheva, E. *Chem. Mater.* **1996**, *8*, 182.
(27) Alcántara, R.; Lavela, P.; Tirado, J. L.; Stoyanova, R.; Gorova, M.; Kuzmanova, E.; Zhecheva, E. In *Batteries for Portable Applications and Electric Vehicles*; Holmes, C. F., Landgrebe, A. R., Eds.; Electrochemical Society: Pennington, NJ, 1997; p 109.

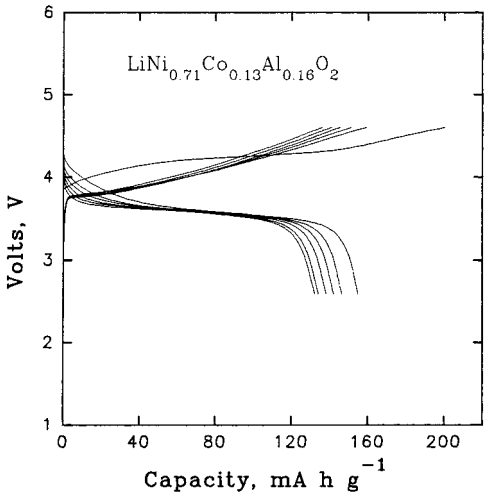

Figure 6. Intensiostatic cycling of $Li/LiClO_4(PC + EC)/LiAl_{0.16}Ni_{0.71}Co_{0.13}O_2$ test cells recorded at C/50.

$Ni_{0.71}Co_{0.13}O_2$ and those reported for $LiAl_yNi_{1-y}O_2$[13] is probably indicative of a cation distribution closer to the latter solid, that is, having Al^{3+} ions in octahedral coordination almost exclusively. This in turn should affect the electrochemical behavior. Figures 5B and 6 show the results of the SPES measurements and galvanostatic cycling of lithium anode cells using this sample as cathode material, respectively. The first potentiostatic cycle in Figure 5B evidences a better reversibility of the lithium extraction−insertion process of $LiAl_{0.16}Ni_{0.71}Co_{0.13}O_2$, as compared with the $Li_xAl_{0.2}Co_{0.8}O_2$ electrode (Figure 5A). The galvanostatic capacity after the first discharge takes a value of 155 mA h g^{-1} for $LiAl_{0.16}Ni_{0.71}Co_{0.13}O_2$ (Figure 6). An excellent capacity retention is also observed for this material during the first cycles. Thus a capacity of ca. 134 mA h g^{-1} is observed after cycle 5, which suffers little change in the following cycles recorded in Figure 6.

Acknowledgment. The authors acknowledge the financial support of CE, Contract JOU2-CT93-0326 and Supplementary Agreement CIPD-CT94-0501. The authors also express their gratitude toward CICYT (Contract PB95-0561) for meeting publication costs, Instituto Andaluz de Química Fina for X-ray diffraction facilities, and Servicio de RMN (Universidad de Córdoba).

IC9707220